



1  
2  
3  
4  
5  
6  
7  
8  
9  
10  
11  
12  
13  
14  
15  
16  
17  
18  
19  
20  
21  
22  
23  
24  
25  
26  
27  
28  
29  
30  
31  
32  
33  
34  
35  
36

## Are drivers of northern lights in the ionosphere?

Office Geophysik, Ogoori, 838-0141, Japan

Osuke Saka

Saka.o@nifty.com

### Abstract

Known as northern lights, auroral spirals are distinct features of substorm auroras composed of large-scale spirals (100s km Surges) mixed with smaller scale ones (10s km Folds, and 1 km Rays). Spiral patterns are generally interpreted in terms of the field line mapping of the upward field-aligned currents produced in the magnetosphere during the field line dipolarization. The field line mapping results in opposing spiral rotations of small- and large-scale auroras. Because of a rotational symmetry deformation and similarity in deformation speeds (6–8 km/s) of small- and large-scale spirals, it has been suggested that common physical processes may underlie the deforming processes. Internal processes in the polar ionosphere (ionospheric driver) will be proposed as the general dynamic for spiral auroras. The ionospheric driver rotated in the ionosphere to produce spirals that characteristically differ from the field line mapping scenario.

### 1. Introduction

Decades of ground-satellite observations of auroras using imagers, magnetometers, and onboard particle and field detectors revealed that a primary driver of auroras associated with the substorms is in the magnetosphere. It has been recently suggested that an arrival of Bursty Bulk Flows [Angelopoulos et al., 1992], Dipolarization Front [Runov et al., 2011], and Plasma Bubbles (low entropy flux tubes) [Sergeev et al., 1996] from the tail may alter convection patterns in the midnight magnetosphere to initiate onset auroras, such as poleward boundary intensification, streamers, beading of the onset arc, and auroral bulge. Spiral forms in the auroral bulge ranging from small spatial scale (Rays, 1 km) to large (Westward Traveling Surges, 100s km) are distinct auroral forms associate with the dipolarization onset. In the magnetospheric driver scenario, auroral forms observed in the polar ionosphere are determined by the field line mapping [Borovsky, 1993; Stenbaek-Nielsen et al., 1999; Forsyth et al., 2020]. Due to a twist of the flux tubes by the upward



37 field-aligned currents, auroral motion in spirals would show counterclockwise rotations  
38 viewed in a direction parallel to the background magnetic fields as proposed by the current  
39 sheet model [Hallinan, 1976; Nikolaev et al., 2015].

40 Meanwhile, negative charge excess, charge sheet deposited by auroral electron  
41 precipitations, or electron beams produced an opposite rotation of the spiral auroras [Oguti,  
42 1974; 1978; Hallinan, 1970]. The charge sheet model was applied to small-scale spirals  
43 (Rays), while large-scale spirals are supposed attributable to the current sheet model  
44 [Hallinan, 1976]. Oguti (1975) however argued that the similar deformation processes  
45 among small and large-scale spirals suggest that general dynamics may produce small to  
46 large scale sizes. Oguti (2010) described spiral auroras in the auroral bulge as a whole “S-  
47 fractal manifold aurora”.

48 To explain consistent rotations from small-scale to large-scale spirals, we propose the  
49 existence of internal processes in polar ionosphere which generate substorm auroras. This  
50 new scenario is referred to as ionospheric injection [Saka, 2019, 2021] and is summarized  
51 in Sect. 2. In Sect. 3, the ionospheric injection scenario will be adopted to explain spatial  
52 scale size, shapes, rotation, growth time, and potential drop associated with the spiral  
53 auroras. In Sect. 4, example of large-scale spirals triggered by the onset of field line  
54 dipolarization is presented. Summary and discussion of this scenario is given in Sect. 5.

55  
56

## 57 **2. Summary of ionospheric injection scenario**

58 The ionospheric injection is first triggered by westward electric fields transmitted from the  
59 convection surge in the magnetosphere in association with dipolarization onset. In the E-  
60 layer, localized westward electric fields yield electron accumulation (negative charge  
61 region) in lower latitudes while ions are left behind (positive charge region) in the higher  
62 latitudes because of differing electron and ion mobility in the E-layer. Local breakdown of  
63 the charge neutrality in the ionosphere may immediately feedback to the magnetosphere  
64 by imposing imbalance in distributions of ions and electrons along the field lines. This  
65 imbalance can be understood by attracting ions (electrons) earthwards and repelling  
66 electrons (ions) tailward along the field lines by the appearance of negatively (positively)  
67 charged regions in the ionosphere. As a result, parallel electric fields directing upward  
68 (downward) are produced along the field lines from negatively (positively) charged regions  
69 in the ionosphere. The evaporations of ions (electrons) from negatively (positively) charged  
70 regions associated with parallel electric fields would interrupt the perfect neutralization of  
71 the ionosphere by the Pedersen currents but achieve quasi-neutral equilibrium of the  
72 ionosphere.



73 Cold plasmas thus evaporated from the polar ionosphere are transported along the  
74 dynamical trajectories to the magnetosphere conserving the total energy (including  
75 electrostatic potentials) and first adiabatic invariant. However, ions/electrons traveling in  
76 accelerating potential gradients lose perpendicular and lower velocities in parallel  
77 component, leaving only the energetic part of ionospheric plasmas collimated along the  
78 field lines. While for ions/electrons traveling in the potential barrier, they do not change  
79 original pitch angle distributions and energies in the ionosphere. In the magnetic mirror  
80 geometry, pitch angle anisotropies of evaporated ions/electrons further develop initial  
81 potential gradients along the field lines. The potential drop would develop to retain sufficient  
82 energies for driving auroral precipitations in low altitude acceleration regions. Auroras are  
83 excited locally in the negatively charged regions, and black auroras are from positively  
84 charged regions in the ionosphere. Negatively charged and positively charged regions in  
85 the ionosphere correspond to electron rich and ion rich regions and are referred to as ion  
86 and electron holes, respectively.

87  
88

### 89 **3. Modeling the northern lights**

90 An auroral sheet expanding in east-west directions appears at the low-latitude end of the  
91 flow channel created by the westward component of transient electric fields. The auroral  
92 sheet can be interpreted as 1-D ion hole along longitudes. Because longitudinal extent of  
93 the sheet is limited, perpendicular electric fields converging in the center of the sheet  
94 develop. Figure 1 depicts amplitude profiles of electrostatic potential ( $\Phi$ ), electric fields  
95 ( $E$ ), and density difference between ions and electrons ( $n_i - n_e$ ) in the sheet.  $X$  denotes a  
96 distance from the center of the sheet. Amplitudes of  $\Phi$ ,  $E$ ,  $n_i - n_e$ , and distance  $X$  are in  
97 arbitrary scale. The sheet ( $-40 < X < 40$ ) is composed of electron rich regions ( $n_e > n_i$ ) in  
98  $-27 < X < 27$  and ion rich walls ( $n_i > n_e$ ) peaked at  $X = -37, 37$ . Total charges of ions and  
99 electrons are balanced in the sheet. The electron rich regions did not uniformly expand but  
100 have two peaks at  $X = -18$  and  $18$ , because converging electric fields transported electrons  
101 towards the ion rich walls at  $X = -37, 37$ , though the velocity was two orders of magnitudes  
102 smaller than the ExB drift at 100km in altitudes [Kelley, 1989]. The profile of the density  
103 difference ( $n_i - n_e$ ) is integrated with  $X$  to calculate electric fields and electrostatic  
104 potentials. It is assumed that this potential structure was retained for some time ( $\sim 1$  min),  
105 because ion holes are continuously produced by the arriving transient electric fields.



106 A winding motion of auroral sheet is calculated in  $-20 < X < 20$  through ExB drift  
107 using convergent electric fields and magnetic fields pointing downward (northern  
108 hemisphere). It is assumed that (1) one dimensional potential profile in Figure 1 is  
109 conserved during the winding motion, (2) the auroral acceleration region follows the motion  
110 of ion holes, (3) there are no auroras in ion rich regions. The results are shown in Figure 2  
111 in which auroral sheet rotated clockwise around the center viewed in a direction parallel to  
112 the background field lines. Auroral sheet developed expanding its length during rotation  
113 and left folding pattern at the center. Growth time of the spiral aurora ( $\Delta t$ ) can be given by,  
114  $\Delta t = r / v$ . Here,  $r$  is scale size of the spiral aurora, and  $v$  is convection velocity defined by  
115 electric field drift. For the small-scale Rays ( $r = 1\text{km}$ ), the growth time could be estimated to  
116 be 0.125 sec for drift velocity of the order of 8 km/s [e.g., Oguti, 1975], while for large-scale  
117 Surges ( $r = 1000\text{km}$ ), the growth time increased to 125 sec (2.1 min) with the same electric  
118 field intensity ( $E = 400\text{mV/m}$  at  $V=8\text{ km/s}$ ). Electric field intensities independent of the scale  
119 size of spiral aurora suggest that the converging electric fields in the auroral sheet are  
120 effectively shielded by the positive potential barriers peaked at  $X = -37, 37$ . For the  
121 converged electric fields with mean amplitudes of the order of 0.2V/m, the potential drop for  
122 the small-scale Rays ( $r = 1\text{km}$ ) could be 100V, while for the large-scale Surges ( $r =$   
123 1000km) the potential drop could be 100kV in the polar ionosphere.

124 The winding forms of the auroral sheet was affected by the potential profiles in auroral  
125 sheet. For the case where electron rich regions have a single peak at the center ( $X = 0$ ),  
126 winding motion that resembled jetting from the rotating nozzle was obtained (not shown).

127  
128

#### 129 **4. Large-scale spirals**

130 An example of large-scale spirals in all-sky image observed at 0331:00 UT 02 Jan 1986 in  
131 northern hemisphere (SHM; 55.9N, 267.9 in geographic coordinates) is presented in Figure  
132 3 (adapted from Saka et al. (2012)). Multiple shear layers constituting the Westward  
133 Traveling Surge extended about 750 km in longitudes and 450 km in latitudes. It developed  
134 in the all-sky image following the onset of field line dipolarization at 0330:36 UT in  
135 magnetometer data at geosynchronous orbit. Shear layers were bounded at poleward  
136 boundary by poleward boundary aurora surge (PBAS) propagating eastward (solid arrow).  
137 Motions of shear layers are consistent with the spiral arms rotating clockwise in poleward  
138 latitudes as shown in Figure 2. Spiral arms in equatorward latitudes were not observed in  
139 this field-of-view. PBAS is an auroral manifestation of the flow shear in the midnight  
140 magnetosphere produced by the onset of field line dipolarization [Saka et al., 2012].

141



142

143 **5. Discussion and Summary**

144 The ionospheric injection scenario adequately explains the clockwise deformation of  
145 auroral arcs in auroral bulge regardless of scale sizes. Parallel electric fields pointing  
146 upward originated from the ion holes would draw upward field-aligned currents. Current  
147 sheet model may not be applicable to the ionospheric injection scenario, because drivers  
148 (ion holes) rotated in the polar ionosphere to produce spiral auroras not subject to field line  
149 mapping. The ionospheric injection scenario is consistent with the charge sheet model,  
150 though ion holes were not produced by the electron beams but rather by the evaporation of  
151 cold ions. The longitudinal scale size of ion holes may be determined by the longitudinal  
152 width of the equatorward flow channels created by the transient electric fields. In large-  
153 scale channels extending 100s km in east-west direction, smaller scale channels may be  
154 embedded to generate meso- and small-scale spirals.

155

156

157 **6. Data availability**

158 No data sets were used in this article.

159

160 **7. Competing interest**

161 The author declares that there is no conflict of interest.

162

163

164

165 **References**

- 166 Angelopoulos, V., Baumjohann, W., Kennel, C.F., Coronitti, F.V., Kivelson, M.G., Pellat, R.,  
167 Walker, R.J., Luhr, H., and Paschmann, G.: Bursty bulk flows in the inner central  
168 plasma sheet, *J.Geophys.res.*, **97**, 4027-4039, 1992.
- 169 Borovsky, J.E.: Auroral arc thickness predicted by various theories, *J.Geophys.Res.*, **98**,  
170 6101-6138, 1993.
- 171 Forsyth, C., Sergeev, V.A., Henderson, M.G., Nishimura, Y., and Gallardo-Lacourt, B.:  
172 Physical processes of meso-scale, dynamic auroral forms, *Space Sci. Rev.* 216:46,  
173 <https://doi.org/10.1007/s11214-020-00665-y>, 2020.
- 174 Hallinan, T.J.: Auroral spirals 2. Theory, *J. Geophys. Res.*, **81**, 3959-3965, 1976.
- 175 Hallinan, T.J., & Davis, T.N.: Small-scale auroral arc distortions. *Planet Space Sci.*, **18**,  
176 1735-1744, 1970.



- 177 Kelley, M.C.: The earth's ionosphere: plasma physics and electrodynamics, Academic  
178 Press, Inc., 1988.
- 179 Nikolaev, A.V., Sergeev, V.A., Tsyganenko, N.A., Kubyshkina, M.V., Opgenoorth, H.,  
180 Singer, H., & Angelopoulos, V.: A quantitative study of magnetospheric field line  
181 deformation by a two-loop substorm current wedge, *Ann. Geophys.*, **33**, 505-517,  
182 2015.
- 183 Oguti, T.: Rotational deformations and related drift motions of auroral arcs. *J. Geophys.*  
184 *Res.*, 3861-3865, 1974.
- 185 Oguti, T.: Similarity between global auroral deformations in DAPP photographs and small  
186 scale deformations observed by a TV camera. *J. Atmos.Terr. Phys.*, **87**, 113-1418,  
187 1975.
- 188 Oguti, T.: Observations of rapid auroral fluctuations, *J. Geomag. Geoelectr.*, **30**, 299-314,  
189 1978.
- 190 Oguti, T.: Introduction to auroral physics (in Japanese), Edited by Solar-Terrestrial  
191 Environment Laboratory, Nagoya University, 2010.
- 192 Runov, A., Angelopoulos, V., Zhou, X.-Z., Zhang, X.-J., Li, S., Plaschke, F., and Bonnell, J.:  
193 A THEMIS multicase study of dipolarization fronts in the magnetotail plasma sheet,  
194 *J.Geophys.Res.*, **116**, A05216, doi:10.1029/2010JA016316, 2011.
- 195 Saka, O., Hayashi, K., and Koga, D.: Periodic aurora surge propagating eastward/westward  
196 at poleward boundary of aurora zone during the first 10 min intervals of Pi2 onset,  
197 *J.Atmos.Solar Terr.Phys.*, **80**, 285-295, 2012.
- 198 Saka, O.: A new scenario applying traffic flow analogy to poleward expansion of auroras,  
199 *Ann. Geophys.* **37**, 381-387, 2019.
- 200 Saka, O.: Ionospheric control of space weather, *Ann. Geophys.* **39**, 455-460, 2021.
- 201 Stenbaek-Nielsen, H.C., Hallinan, T.J., and Peticolas, I.: Why do auroras look the way they  
202 do?, *Eos*, **80**, 193-204, 1999.
- 203  
204  
205  
206  
207  
208  
209  
210  
211  
212

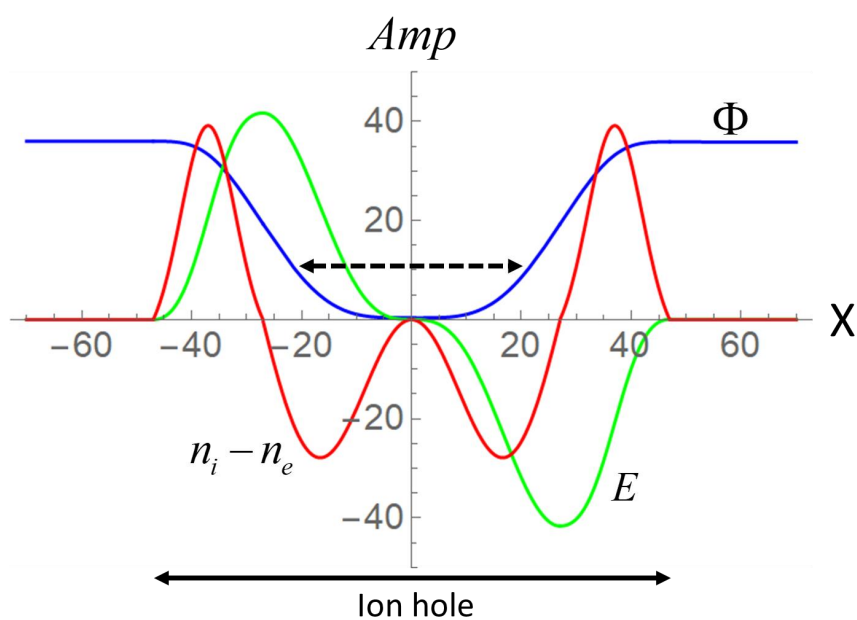


**Figure 1**

213 Distribution of electrostatic potentials ( $\Phi$ , blue), electric fields ( $E$ , green), and density  
214 difference between ions and electrons ( $n_i - n_e$ , red) in one dimensional ion hole model.  $X$  is  
215 positive eastward. Winding motion of the negative potential region marked by dotted arrow  
216 is shown in Figure 2. See text for details.

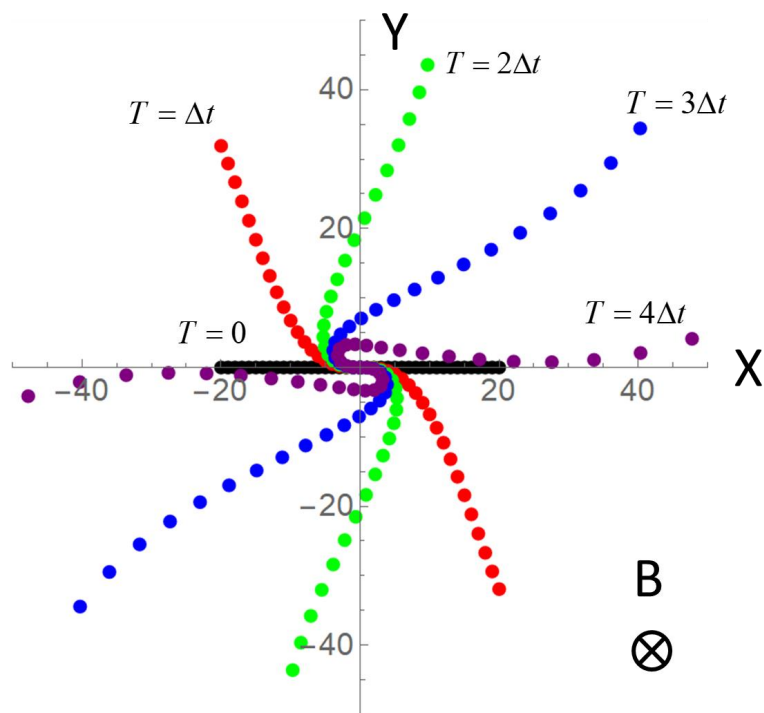


**Figure 2**

217 The auroral sheet initially in the east-west directions in black ( $T=0$ ) deformed to red ( $T=\Delta t$ ),  
218 green ( $T=2\Delta t$ ), blue ( $T=3\Delta t$ ), and to purple ( $T=4\Delta t$ ) in X-Y plane. X is east and Y is north.  
219 The  $E \times B$  drift rotated each element of the auroral sheet represented by dots clockwise  
220 viewed in a direction parallel to the background field lines. Direction of magnetic fields is  
221 into the page.



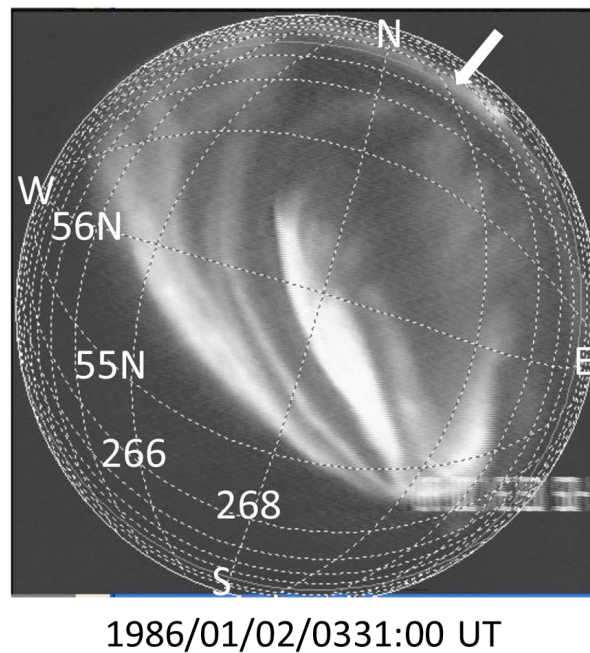


**Figure 3**

222 All-sky image viewed from above the ionosphere for dipolarization event taken at 0331:00  
223 UT in northern hemisphere, following the dipolarization spike at 0330:36 UT at  
224 geosynchronous orbit. Grids in the image are geographic longitudes and latitudes, nearly  
225 parallel to the geomagnetic coordinates. Grid separation 2 degrees in longitudes is 125 km  
226 along 56N and 112 km for one degree in latitudes. Poleward arrow denotes PBAS. See text  
227 for details.